Pivotal role of cardiomyocyte TGF-β signaling in the murine pathological response to sustained pressure overload

Norimichi Koitabashi,[1] Thomas Danner,[1] Ari L. Zaiman,[2] Yigal M. Pinto,[3] Janelle Rowell,[1] Joseph Mankowski,[4] Dou Zhang,[1] Taishi Nakamura,[1] Eiki Takimoto,[1] and David A. Kass[1]

[1]Division of Cardiology and [2]Division of Pulmonary and Critical Care Medicine, Department of Medicine, Johns Hopkins Medical Institutions, Baltimore, Maryland, USA. [3]Heart Failure Research Center, University of Amsterdam, Amsterdam, The Netherlands. [4]Division of Comparative Medicine, Johns Hopkins Medical Institutions, Baltimore, Maryland, USA.

The cardiac pathological response to sustained pressure overload involves myocyte hypertrophy and dysfunction along with interstitial changes such as fibrosis and reduced capillary density. These changes are orchestrated by mechanical forces and factors secreted between cells. One such secreted factor is TGF-β, which is generated by and interacts with multiple cell types. Here we have shown that TGF-β suppression in cardiomyocytes was required to protect against maladaptive remodeling and involved noncanonical (non–Smad-related) signaling. Mouse hearts subjected to pressure overload and treated with a TGF-β–neutralizing Ab had suppressed Smad activation in the interstitium but not in myocytes, and noncanonical (TGF-β–activated kinase 1 [TAK1]) activation remained. Although fibrosis was greatly reduced, chamber dysfunction and dilation persisted. Induced myocyte knockdown of TGF-β type 2 receptor (TβR2) blocked all maladaptive responses, inhibiting myocyte and interstitial Smad and TAK1. Myocyte knockdown of TβR1 suppressed myocyte but not interstitial Smad, nor TAK1, modestly reducing fibrosis without improving chamber function or hypertrophy. Only TβR2 knockdown preserved capillary density after pressure overload, enhancing BMP7, a regulator of the endothelial-mesenchymal transition. BMP7 enhancement also was coupled to TAK1 suppression. Thus, myocyte targeting is required to modulate TGF-β in hearts subjected to pressure overload, with noncanonical pathways predominantly affecting the maladaptive hypertrophy/dysfunction.

Introduction

Heart disease is the frequent consequence of longstanding neurohormonal and mechanical stress and, despite recent advances, remains a leading cause of death worldwide among older adults (1). Pathological stress, as from hypertension, stimulates a broad array of molecular signaling cascades (2–4), resulting in chamber dilation, hypertrophy, dysfunction, interstitial fibrosis, and altered microvascular structure (5, 6). Both cardiac muscle and interstitial cells are involved in the pathophysiology, and each has become a therapeutic target. Growing evidence supports a key role for crosstalk between these compartments that involves mechanical and electrical coupling as well as chemical interactions from a variety of secreted factors. A prominent example of the latter is TGF-β (7, 8), which is expressed by and modulates myocytes, vascular cells, and fibroblasts (7, 9). Its expression rises in myocardium in experimental and human heart disease (9–11), and it promotes hypertrophy, fibrosis, apoptosis, and endothelial-mesenchymal transition (12, 13). The distal signaling coupled to TGF-β activation is complex, differing among cell types; perhaps as a result, its role in heart disease pathophysiology has remained ambiguous.

TGF-β signals via a classical pathway, binding to TGF-β type 2 receptor (TβR2; encoded by *TGFBR2*) to activate TGF-β type 1 receptor (TβR1; encoded by *TGFBR1*, also referred to as *ALK5*) and subsequently Smad transcription factors (notably Smad2/3; refs. 12, 14, 15). Noncanonical (Smad-independent) signaling involving direct kinase activation also occurs (14), and among its targets, TGF-β–activated kinase 1 (TAK1) appears important to heart disease (16). Myocyte TGF-β stimulation induces hypertrophy (17, 18), whereas mice lacking TGF-β1 display blunted angiotensin II–mediated cardiac hypertrophy (19). Blockade from TGF-β–neutralizing Abs (N-Abs) has gained prominence from studies of arterial and skeletal myopathies in Marfan syndrome (20, 21). However, in stressed hearts, such inhibitors have had less impact on hypertrophy or systolic dysfunction, and they may worsen chamber dilation (22–24). The cause for this disparity is unknown, but could relate to the cascade and/or the cell types targeted. Mice with systemic Smad3 knockout develop more hypertrophy yet less fibrosis in response to pressure overload (25), whereas myocyte-specific TAK1 overexpression stimulates hypertrophy and heart failure (16). Given that TGF-β signaling differs among cell types and environments (15), cell-selective conditional gene manipulation is needed to dissect its role. Here, we reveal prominent and highly protective effects against pressure overload stress in hearts with induced gene suppression of myocyte TβR2, whereas N-Ab treatment blocking interstitial but not myocyte TGF-β signaling worsened the response. Comparison of myocyte TβR2 versus myocyte TβR1 knockdown suggested that noncanonical TGF-β signaling coupled to TAK1 is particularly important in maladaptive hypertrophy and myocardial dysfunction caused by chronic pressure overload.

Results

Pressure overload induces late activation of TGF-β signaling. Sustained pressure overload was induced in mice by means of transverse aortic constriction (TAC). In our model, this results in concentric hypertrophy of the LV by 1 week, followed by progressive cardiac

Conflict of interest: The authors have declared that no conflict of interest exists.
Citation for this article: *J Clin Invest.* 2011;121(6):2301–2312. doi:10.1172/JCI44824.

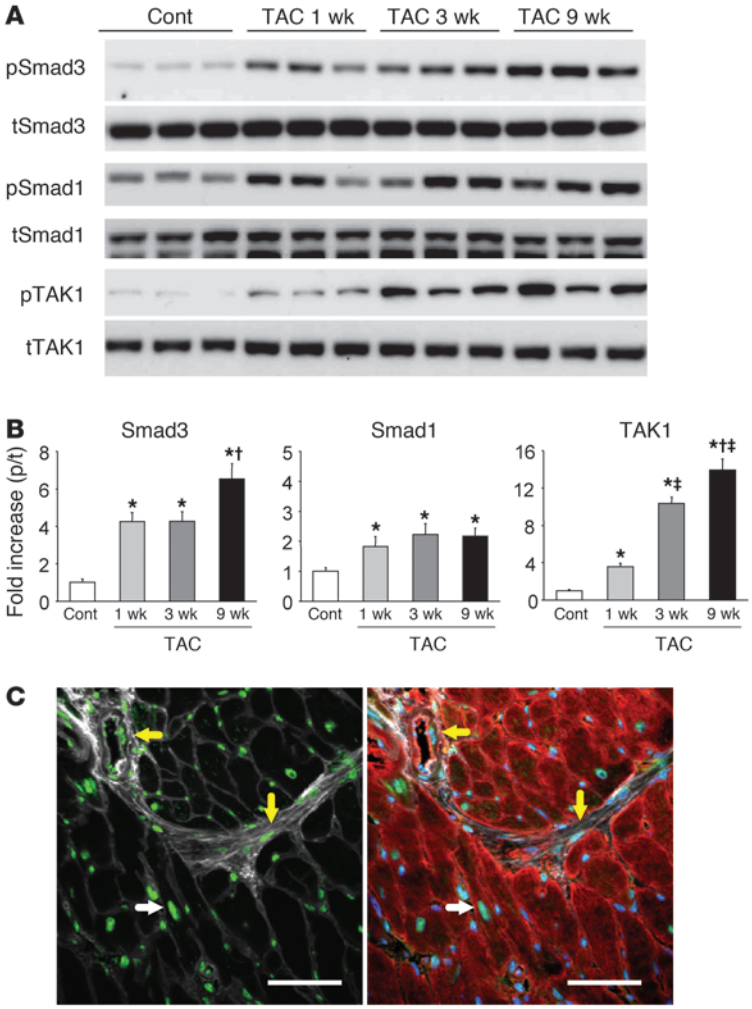

Figure 1
Smad3 and TAK1 phosphorylation are increased in chronic phases of pressure overload. (**A**) Representative Western blot for phosphorylated (p-) and total (t-) Smad3, Smad1, and TAK1 using LV tissue lysates after TAC. Cont, sham control. (**B**) Summary data for immunoblot. $n = 4–6$. $^{*}P < 0.05$ vs. sham; $^{\dagger}P < 0.05$ vs. 3-week TAC; $^{\ddagger}P < 0.05$ vs. 1-week TAC. (**C**) Immunostaining for phospho-Smad3 (green) in 9-week TAC LV myocardium. Blue, DAPI (nucleic acid); red, sarcomeric α-actinin (myocytes); white, WGA (membrane/extracellular matrix). White arrows, cardiomyocyte Smad3 activation; yellow arrows, nonmyocyte (e.g., fibroblast, vascular SMC) Smad3 activation. Scale bars: 50 μm.

dilation and, ultimately, failure (26, 27). Interstitial fibrosis develops early and worsens with decompensation (26, 27). As shown in Figure 1, A and B, this was also accompanied by gradual TGF-β activation, reflected by both Smad3 and TAK1 phosphorylation. Temporal changes of TAK1 phosphorylation paralleled those for Smad3, whereas Smad1 phosphorylation rose early and remained enhanced throughout (Figure 1, A and B). Smad2 phosphorylation also rose, but unlike Smad3, this occurred in parallel with total protein expression; Smad4 expression was unchanged (Supplemental Figure 1A; supplemental material available online with this article; doi:10.1172/JCI44824DS1). Given these results, we used phospho-Smad3 changes to reflect canonical signaling. Confocal immunohistochemistry revealed that after 9 weeks of TAC, phospho-Smad3 nuclear localization (i.e., activation) was detected in multiple cell types, including myocytes, vascular SMCs, endothelial cells, and cardiac fibroblasts (Figure 1C).

Systemic inhibition of TGF-β fails to suppress cardiac pathological remodeling. TAC mice were systemically administered a monoclonal N-Ab neutralizing TGF-β1–TGF-β3 activity (24, 28) or control Ab (C-Ab). N-Ab treatment did not improve heart function, and actually worsened chamber dilation (Figure 2, A and B, and Supplemental Table 1). Although increases in cardiac hypertrophy and myocyte size were similar in the N-Ab and C-Ab treatment groups (Figure 2, C and D), mice receiving N-Ab displayed markedly suppressed interstitial and perivascular fibrosis (Figure 2, E and F).

The failure of N-Ab to alter myocardial structure and function despite its effective suppression of fibrosis suggested that the treatment may have primarily targeted interstitial TGF-β. Overall myocardial phospho-Smad3 was indeed suppressed by N-Ab treatment (Figure 3A), although activation of TAK1, a kinase predominantly expressed in myocytes (29), was unaltered. Importantly, confocal immunofluorescence revealed that nuclear phospho-Smad was markedly suppressed in SMCs (Figure 3, B and C) and cardiac fibroblasts (Figure 3, D and E), but myocyte activation remained. The hypothesis that the N-Ab primarily targeted interstitial cells was further supported by injection of an Alexa Fluor 555–labeled N-Ab that colocalized with the macrophage marker CD68 (Supplemental Figure 1B). Expression of the myocyte hypertrophy fetal marker genes atrial natriuretic peptide (*Nppa*), brain natriuretic peptide (*Nppb*), and β–myosin heavy chain (*Myh7*) were all enhanced by TAC and unchanged by N-Ab treatment (Figure 3F). Expression of myocyte-derived connective tissue growth factor (*Ctgf*), which is downstream of TGF-β activation (30), also remained elevated, whereas expression of periostin (*Postn*), a fibroblast specific TGF-β–coupled gene (31), declined with N-Ab treatment (Figure 3F).

Cardiomyocyte-specific TβR2 knockdown prevents maladaptive remodeling in response to pressure overload. Since N-Ab neither antagonized myocyte TGF-β signaling nor countered myocyte-derived maladaptive gene expression, we hypothesized that targeting these cells might be particularly important to the hypertrophy and dysfunction that ensues from sustained pressure overload. To test this, we generated MCM$^{+/-}$*Tgfbr2*$^{fl/fl}$ mice, with tamoxifen-inducible TβR2 conditional knockdown (cKD) in cardiomyocytes only (referred to herein as TβR2^{cKD} mice). These animals expressed a floxed *Tgfbr2* gene and myocyte-specific tamoxifen-inducible *Cre* (MerCreMer [MCM]; ref. 32), as global *Tgfbr2*$^{-/-}$ is embryonic lethal (33). As the MCM model can exhibit transient, reversible cardiomyopathy (32), we used 2 additional controls, MCM$^{+/-}$ no-flox and MCM$^{-/-}$ *Tgfbr2*$^{fl/fl}$ (referred to herein as MCM and TβR2^{FF}, respectively), and delayed subjecting hearts to TAC until at least 3 weeks after tamoxifen administration, when cardiac function and molecular signaling normalizes (32). The model resulted in approximately 80% knockdown in TβR2, with no change in TβR1 (Supplemental Figure 1C and ref. 32). In marked contrast to the results with N-Ab, TβR2^{cKD}

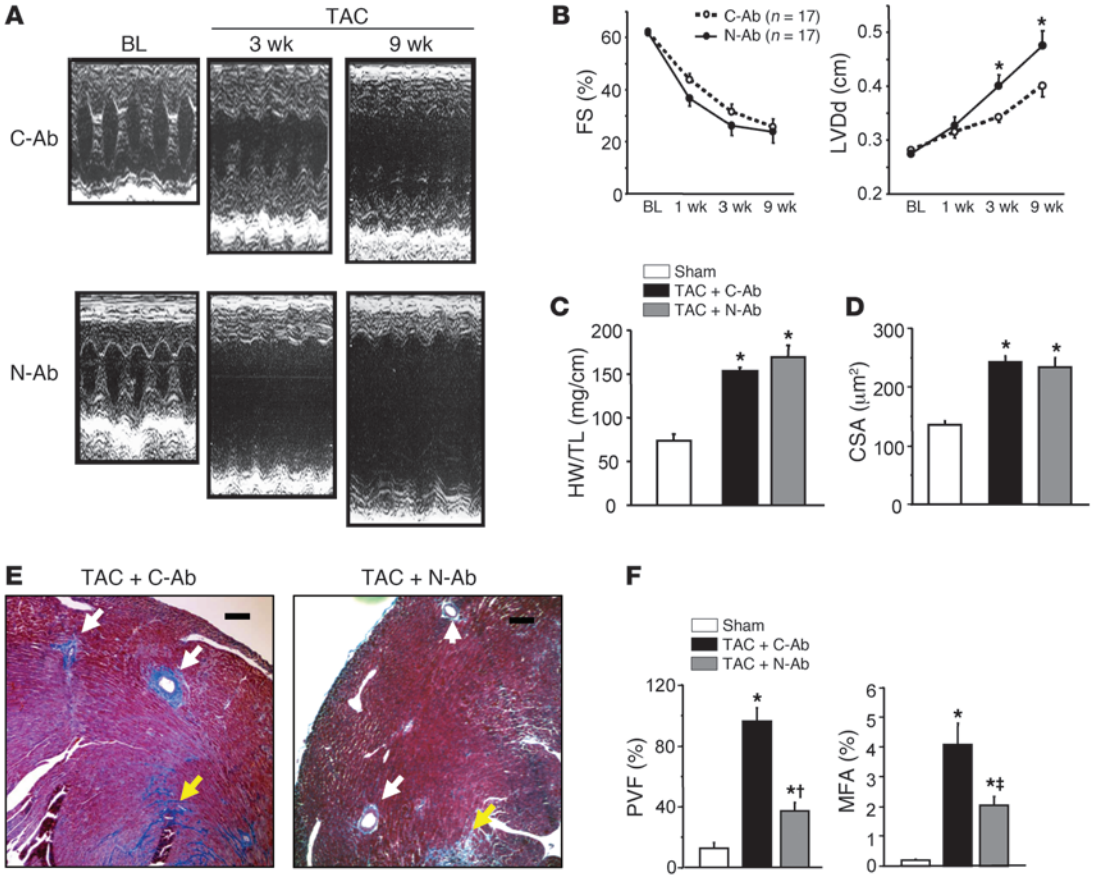

Figure 2
Effect of TGF-β N-Ab on cardiac response to TAC. (**A** and **B**) Temporal changes of FS and LV diastolic dimension (LVDd). *$P < 0.05$ vs. C-Ab, ANOVA. BL, baseline. (**C**) Heart weight/tibia length ratio (HW/TL). $n = 10$ (sham); 17 (TAC plus C-AB and TAC plus N-Ab). *$P < 0.05$ vs. sham. (**D**) Averaged cardiomyocyte cross-sectional area (CSA) obtained by WGA staining, 500–800 cells per heart, 10 hearts per group. *$P < 0.05$ vs. sham. (**E**) Representative Masson trichrome staining. White arrows, perivascular fibrosis; yellow arrows, interstitial fibrosis. N-Ab treatment markedly suppressed perivascular fibrosis. Scale bars: 100 μm. (**F**) Summary results for perivascular fibrosis area (PVF) and myocardial fibrosis area (MFA). $n = 8$ (sham); 17 (TAC plus C-Ab and TAC plus N-Ab). *$P < 0.05$ vs. sham; †$P < 0.001$, ‡$P < 0.05$ vs. TAC plus C-Ab.

mice were well protected against TAC-induced remodeling, developing neither dilation nor chamber dysfunction and displaying improved heart function despite persistent increased afterload (Figure 4, A–D, and Supplemental Table 2). Whole-heart and myocyte hypertrophy were significantly lower (Figure 4, E–G).

Intriguingly, although TβR2^{cKD} mice only had myocyte TGF-β signaling suppressed, interstitial fibrosis was also markedly diminished (Figure 5, A and B). However, unlike N-Ab–treated hearts, perivascular fibrosis remained unaltered. Confocal imaging revealed a marked decline in myocyte phospho-Smad3 activation as well as suppression in interstitial cells (Figure 5C; compare with Figure 1C). Immunoblot revealed suppression of both phospho-Smad3 and phospho-TAK1 in TβR2^{cKD} myocardium (Figure 5D), and, in further contrast to N-Ab responses, hypertrophy fetal gene upregulation was now suppressed (Figure 5E). Gene induction of both *Ctgf* and *Postn* was attenuated. We further performed a broad analysis of TGF-β–regulated genes by PCR array (Supplemental Table 3) and found that many components of Smad-dependent (e.g., procollagen) and Smad-independent (e.g., cyclin-dependent kinase inhibitor 2b; ref. 34) signaling were induced by TAC in the controls: all were markedly suppressed in TβR2^{cKD} animals.

To directly test that suppression of canonical and noncanonical TGF-β signaling was indeed genetically targeted to myocytes and not fibroblasts in these hearts, both cell types were freshly cultured overnight and exposed to recombinant human TGF-β1 (rhTGF-β1) or vehicle control for 30 minutes (Figure 6A). Control cells showed phosphorylation of Smad3, TAK1, and the downstream target of TAK1, p38 MAPK. MAPK kinase 3/6 (MKK3/6) was also activated (data not shown). None of these proteins was phosphorylated in myocytes from TβR2^{cKD} hearts. In contrast, both control and TβR2^{cKD} fibroblasts exhibited identically increased phospho-Smad3 with TGF-β1 stimulation, pTAK1 was undetectable, and there was no significant change in p38 MAPK phosphorylation. This confirmed the selectivity of cell type targeting in the TβR2^{cKD} model and also indicated that changes in noncanonical signaling at the whole-heart level were most likely derived from myocytes.

We next asked whether TGF-β1 stimulation of myocyte TAK1 could trigger activation of connective tissue–regulating genes and whether this is suppressed by TAK1 inhibition. Cultured adult mouse cardiomyocytes from control hearts showed a greater than 2-fold induction of *Ctgf* expression when stimulated by rhTGF-β1, and this was absent in cells lacking TβR2 (Supplemental Figure 2A).

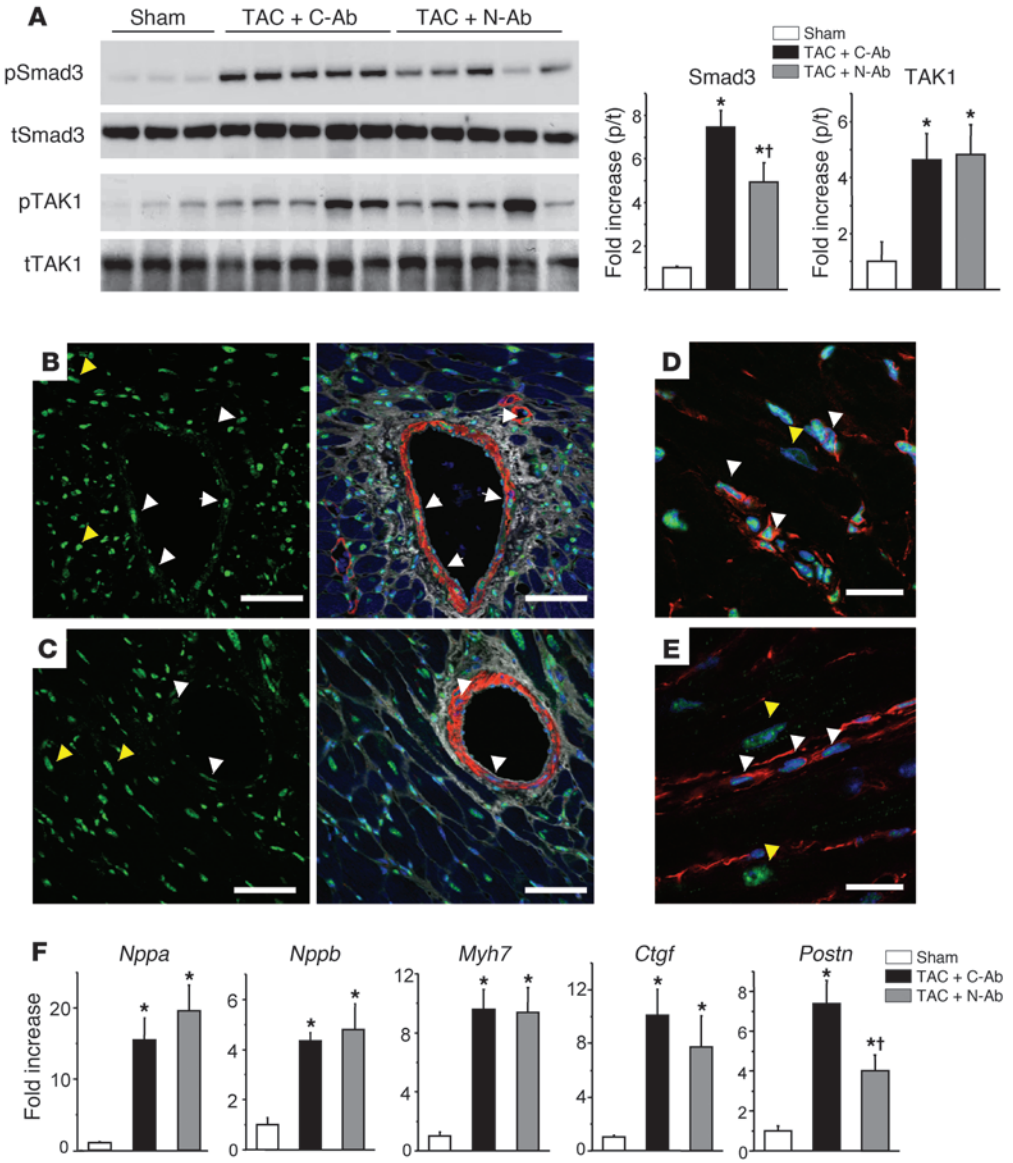

Figure 3
N-Ab suppresses Smad activation in noncardiomyocytes. (**A**) Western blot for Smad3 and TAK1 phosphorylation in 9-week TAC myocardium with N-Ab or C-Ab. Summary data shows reduced activation of Smad3, but not TAK1. $n = 6$ per group. *$P < 0.01$ vs. sham; †$P < 0.05$ vs. TAC plus C-Ab. (**B**–**E**) Phospho-Smad3 immunostaining (green) in 9-week TAC myocardium treated with C-Ab (**B** and **D**) and N-Ab (**C** and **E**). Scale bars: 50 μm. (**B** and **C**) Smad3 activation in vascular SMCs was suppressed by N-Ab treatment. Red, SMA (SMCs); blue, DAPI; white, WGA. White arrows, SMC Smad3 activation; yellow arrows, cardiomyocyte Smad activation. (**D** and **E**) Smad3 activation in cardiac fibroblasts was suppressed by N-Ab. Red, vimentin (cardiac fibroblasts); blue, DAPI. White arrows, fibroblast Smad3 activation; yellow arrows, cardiomyocyte Smad3 activation. (**F**) mRNA expression, normalized to *Gapdh* and then to sham data, assessed by real-time RT-PCR. $n = 4$ (sham); 10 (TAC plus C-Ab and TAC plus N-Ab). *$P < 0.01$ vs. sham; †$P < 0.05$ vs. TAC plus C-Ab.

Importantly, substantial reduction was also observed by treating cells with the TAK1 inhibitor oxozeaenol (Supplemental Figure 2B). Oxozeaenol also suppressed expression of *Nppa* and *Nppb* induced by TGF-β1 (Supplemental Figure 2C), supporting the role of TAK1 in hypertrophic remodeling. Oxozeaenol inhibition of TAK1 was confirmed by suppression of p38 MAPK phosphorylation induced by TGF-β1 (Supplemental Figure 2D).

To further assess whether the lack of myocyte TGF-β targeting by N-Ab could indeed explain its failure to blunt cardiac dilation/dysfunction and hypertrophy from TAC, TβR2^{cKD} mice and control mice were exposed to 3 weeks of TAC with or without coadministration of N-Ab. Administration of N-Ab again led to reduced fractional shortening (FS), greater cardiac dilation, slightly higher estimated LV mass, and reduced fibrosis (Figure 6, B–E). However, N-Ab administered to TβR2^{cKD} mice had less of a negative impact (Figure 6, B–E), essentially behaving much like the TβR2^{cKD} model itself. This finding supports a key role of myocyte TGF-β signaling in the maladaptive responses to TAC.

TβR1^{cKD} mice do not replicate the TβR2^{cKD} response. Canonical TGF-β signaling is initiated by TβR2 activation, resulting in TβR1 and consequent Smad stimulation. Deletion of both TβR1 and TβR2 suppresses TGF-β–mediated Smad2/3 activation in isolated cardiomyocytes (32), but targeting solely TβR1 would not necessarily suppress TAK1 activation (35). To probe the relative importance of non–Smad-dependent (e.g., TAK1) activation, we performed studies in TβR1^{cKD} mice, which displayed approximately 80% decline in TβR1 and unaltered TβR2 (Supplemental Figure 1C). Isolated myocytes from TβR1^{cKD} hearts displayed complete inhibition of myocyte Smad3 activation upon stimulation with TGF-β (Supplemental Figure 3A). Unlike TβR2^{cKD} mice, TAC induced similar cardiac dilation and dysfunction in TβR1^{cKD} mice and increased heart mass and myocyte size compared with those of the various control groups (Figure 7, A–E). Invasive pressure-volume (PV) loop analysis showed an intermediate response in some parameters, although load-independent indexes of systolic function were not different from those of controls (Supplemental Table 2).

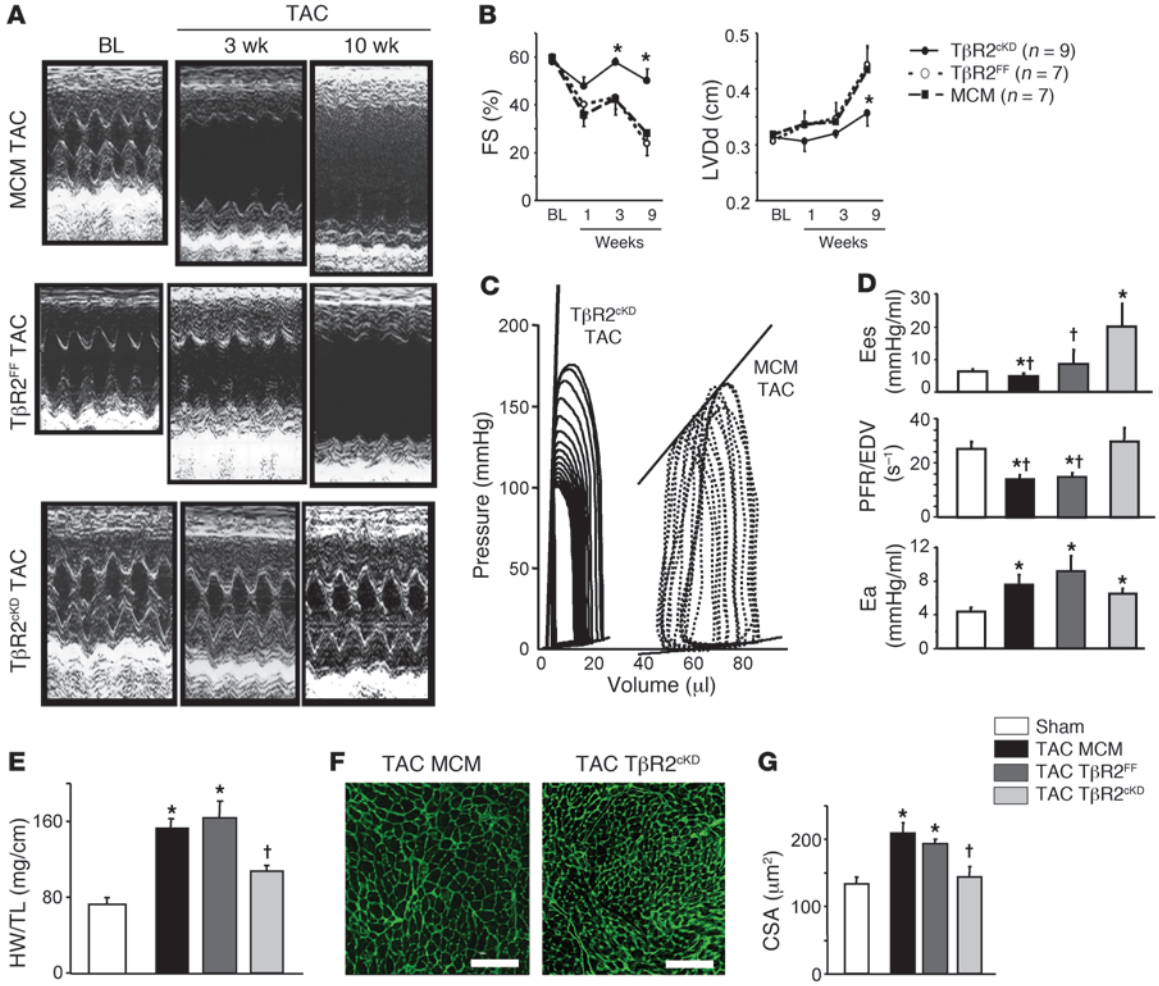

Figure 4

TβR2^{cKD} model displays markedly suppressed cardiac hypertrophy and remodeling after TAC. (**A**) Representative M-mode echocardiogram after TAC. (**B**) Temporal changes of FS and LV diastolic dimension. *P < 0.05 vs. MCM and TβR2^{FF}. (**C** and **D**) Cardiac function, assessed by PV loops, was improved in TβR2^{cKD} animals. (**C**) Representative PV loop. (**D**) Summary data for end-systolic elastance (Ees), as a measure of contractility, peak filling rate/EDV (PFR/EDV), as a measure of diastolic function, and arterial elastance (Ea), as a measure of afterload. n = 4–7 per group. *P < 0.05 vs. sham; †P < 0.05 vs. TβR2^{cKD}; 1-way ANOVA, Tukey test. (**E**–**G**) Cardiac hypertrophy was inhibited in TβR2^{cKD} animals. *P < 0.05 vs. sham (all genotypes); †P < 0.05 vs. TAC MCM and TAC TβR2^{FF}. (**E**) Heart weight/tibia length ratio. n = 8 (sham); 11 (TAC MCM); 6 (TAC TβR2^{FF}); 9 (TAC TβR2^{cKD}). (**F**) Representative WGA staining for CSA measurement. Scale bars: 100 μm. (**G**) Myocyte hypertrophy, as assessed by CSA. Averaged data from 400–800 cells per heart. n = 4 (sham); 7 (TAC MCM); 5 (TAC TβR2^{FF} and TAC TβR2^{cKD}).

In contrast, myocardial fibrosis declined, albeit to a lesser degree than that observed with the TβR2^{cKD} group, whereas increased perivascular fibrosis remained unaltered (Figure 7E). Immunoblots of 9-week TAC LV myocardium showed persistently increased phospho-Smad3, even though myocyte signaling was suppressed (Figure 7F). This disparity was consistent with selective suppression of myocyte but not interstitial cell phospho-Smad3, as revealed by confocal immunohistochemistry (Figure 7G). Myocardial phospho-Smad2 was also not influenced in this model (data not shown). Unlike TβR2^{cKD} hearts, TAK1 activation persisted in TβR1^{cKD} hearts (Figure 7F).

Consistent with this chamber histology and morphology, *Nppa*, *Nppb*, and *Myh7* remained upregulated in TβR1^{cKD} mice, whereas *Ctgf* and *Postn* gene induction significantly declined (Figure 7H). The presence of persistent TAK1 activation in TβR1^{cKD} but not TβR2^{cKD} mice was further explored by assessing MKK3/6 and p38 MAPK in hearts subjected to 3 weeks of TAC. Activation of both declined with TβR2^{cKD} hearts, but not TβR1^{cKD} hearts (Supplemental Figure 3B). At this time point, we also observed a decline in phospho-Smad3 in the TβR1^{cKD} model, separating this from unaltered noncanonical signaling (Supplemental Figure 3B).

Preservation of myocardial capillary density in the TβR2^{cKD} model, but not TβR1^{cKD} or N-Ab models. Recent studies suggest that maladaptive remodeling in the presence of pressure overload is coupled to a decline in adequate vascular supply (36). We therefore examined whether capillary density is affected by any of the 3 methods for modulating cardiac TGF-β signaling. As shown in Figure 8, capillary density normalized to mean myocyte area declined after TAC in control, N-Ab treated, and TβR1^{cKD} hearts. In contrast, this density was preserved in TβR2^{cKD} hearts.

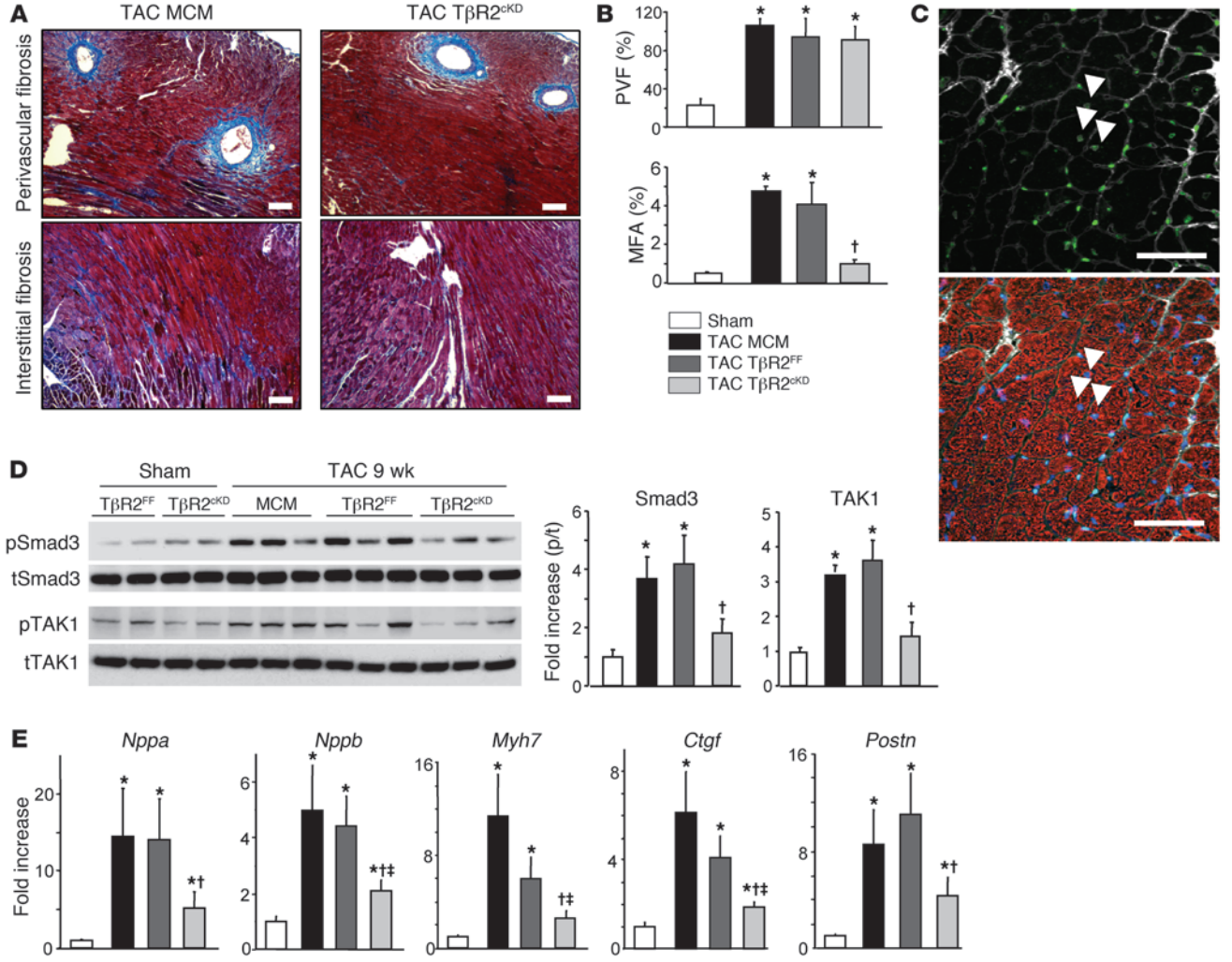

Figure 5

Interstitial fibrosis, but not perivascular fibrosis, is inhibited in the TβR2^{cKD} model. (**A**) Representative Masson trichrome staining in 9-week TAC. Scale bars: 100 μm. (**B**) Summary results for perivascular fibrosis area and myocardial fibrosis area. n = 7 (sham); 11 (TAC MCM); 6 (TAC TβR2^{FF}); 9 (TAC TβR2^{cKD}). *P < 0.05 vs. sham, †P < 0.05 vs. TAC TβR2^{FF} and TAC MCM. (**C**) Phospho-Smad3 immunostaining (green) in 9-week TAC myocardium of TβR2^{cKD} mouse. White arrowheads, cardiomyocyte Smad3 activation. (**D**) Representative Western blot for Smad3 and TAK1 after TAC showed suppression with TβR2^{cKD} mice. Summary results are also shown (n = 5 per group). *P < 0.05 vs. sham; †P < 0.05 vs. TAC TβR2^{FF} and TAC MCM. (**E**) mRNA expression, normalized to *Gapdh* and then to sham data. n = 7 (sham); 4 (TAC MCM); 5 (TAC TβR2^{FF}); 8 (TAC TβR2^{cKD}).*P < 0.05 vs. sham, †P < 0.05 vs. TAC TβR2^{FF}, ‡P < 0.05 vs. TAC MCM.

Modulation of bone morphogenetic protein 7 (BMP7) by myocyte TβR2 signaling. Myocardial fibrosis in response to various stresses has been linked to endothelial-to-mesenchymal cell transition, stimulated by TGF-β1 (13). This change, which may also compromise vascular supply, is countered by another member of the TGF-β superfamily, BMP7. Upregulation of BMP7 suppresses fibrosis and improves function in hearts subjected to pressure overload (13, 37). BMP7 is regulated at the gene expression level (38), and in our PCR array analysis for TGF-β–related signaling, we found *Bmp7* expression both declined after TAC and was the dominant upregulated gene (>4-fold) in TβR2^{cKD} hearts (Supplemental Tables 3 and 4). This was confirmed by real-time RT-PCR (Figure 9A), although the same response was not observed in TβR1^{cKD} hearts. To more directly test the link between myocyte TGF-β1 stimulation and BMP7, cultured neonatal rat ventricular myocytes were transfected with siRNA against either TβR1 or TβR2 (Figure 9, B–D), and *Bmp7* expression was determined upon stimulation with rhTGF-β1. siRNA targeting each respective TGF-β receptor yielded effective knockdown in cultured myocytes (Figure 9, B and C). TGF-β stimulation declined *Bmp7* gene expression significantly in controls and TβR1^{cKD} cells, but not TβR2^{cKD} cells (Figure 9D). This signaling was also examined in cultured adult cardiomyocytes from control or TβR2^{cKD} hearts, and *Bmp7* expression declined only in the controls (Figure 9E). We next tested whether noncanonical signaling via TAK1 could explain the fall in *Bmp7* expression. Control adult myocytes were stimulated with rhTGF-β1 in the presence or absence of the TAK1 inhibitor oxozeaenol. The decline in *Bmp7* was prevented by coinhibition of TAK1 (Figure 9F). This was further confirmed by protein expression analysis showing that TAK1 inhibition prevented the decline in BMP7 protein without altering phospho-Smad3 (Figure 9G).

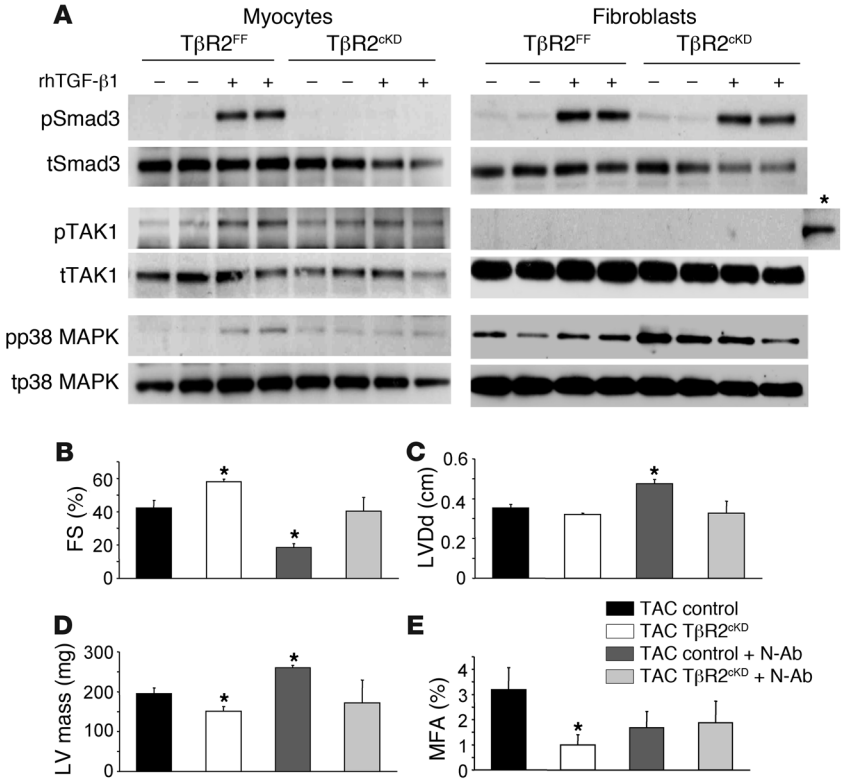

Figure 6
Cardiomyocyte TβR2 knockdown inhibits TGF-β–mediated Smad3 and TAK1 pathways and compensates TGF-β N-Ab–mediated cardiac dysfunction. (**A**) Representative Western blots for Smad3, TAK1, and its downstream target, p38 MAPK, using cultured adult mouse cardiomyocytes and cardiac fibroblasts with or without rhTGF-β1 (5 ng/ml, 20 minutes stimulation). TAK1 phosphorylation could not be detected in cultured adult cardiac fibroblasts. A positive control band from wild-type adult mouse heart lysate is also shown (asterisk). (**B**–**D**) Summarized echo data of 3-week TAC. (**B**) FS. (**C**) LV diastolic dimension. (**D**) Estimated LV mass. $n = 4$ per group (control group contains 2 MCM and 2 TβR2^{FF}). (**E**) Myocardial fibrosis area, estimated by Masson trichrome staining. *$P < 0.05$ vs. control.

Discussion

TGF-β signaling is remarkably diverse, affecting development, morphogenesis, cell survival, growth, and proliferation. Since the peptide acts in both a paracrine and autocrine manner, communication among cells can be critical to determining the net response to its activation or suppression. In the heart, TGF-β regulates fibroblast activation and proliferation, and thus net fibrosis, and methods to suppress its signaling — whether N-Abs or Smad3 deletion — block fibrosis in vitro and in vivo (12, 22, 25). However, these same interventions can be ineffective at ameliorating myocyte hypertrophy and dysfunction (24, 25). The present findings revealed that both cell type– and pathway-specific features of TGF-β signaling were central to understanding this discrepancy. To our knowledge, the TβR2^{cKD} model reveals the most potent impact of TGF-β suppression on modulating cardiac stress remodeling yet reported, effectively blocking myocyte and interstitial maladaptive changes that were otherwise observed in response to sustained pressure overload. Other approaches bypassing myocyte TβR2 signaling proved to be less effective or ineffective.

All 3 methods to suppress TGF-β signaling reduced fibrosis, yet this was insufficient to convey functional or remodeling benefits. This is important, as fibrosis is generally presumed to confer detrimental effects particularly on diastolic function, although this conclusion is often based on indirect guilt by association. It is interesting that both interstitial and perivascular fibrosis were blunted in N-Ab–treated hearts, whereas only interstitial fibrosis was affected in TβR2^{cKD} and TβR1^{cKD} hearts. This likely reflects the circumscribed Ab penetration limiting myocyte interactions. Only when N-Ab was combined with targeted reduction of myocyte TβR2-coupled signaling did post-TAC heart function improve and hypertrophy decline. Perivascular fibrosis from TGF-β stimulation might actually be useful to help coronary arteries adapt to higher perfusion pressures with TAC, although this remains unproven. The fact that interstitial fibrosis declined despite only having myocyte TβR2 (and to a less extent TβR1) reduced identifies these cells as key coordinators of the interstitium via TGF-β–dependent cascades. Although TGF-β secreted by and/or targeted to nonmyocytes was not directly interfered with, phospho-Smad3 was suppressed in these cells when myocyte TβR2 expression was reduced. This was less so with the TβR1^{cKD} model, which indicates that Smad-independent myocyte signaling plays an important role in this cross-talk.

Our results highlighted 2 potential, if not likely, candidates for myocyte-derived communicators, CTGF and BMP7. CTGF is one of several primary factors thought to regulate myofibroblast differentiation and persistence (39), and it can also contribute to hypertrophic stimulation and myocyte dysfunction (40, 41). Here we revealed that TGF-β1 stimulation of CTGF in adult cardiomyocytes is substantially coupled to TAK1 activation, rather than being solely driven by Smad transcriptional regulation. BMP7 has been shown to negatively modulate TGF-β–stimulated fibrosis and endothelial-mesenchymal transition (13), and it can stimulate angiogenesis (42). The current data, for the first time to our knowledge, showed the reverse interaction: TGF-β1 stimulation suppressed myocyte BMP7 by a TAK1-dependent pathway. The relative importance of TAK1 (noncanonical pathway) is further supported by the persistent decline in *Bmp7* for both TβR1^{cKD} and N-Ab models, in which TAK1 was not suppressed. Similarly, *Ctgf* remained elevated in the N-Ab model and declined to a lesser extent in TβR1^{cKD} versus TβR2^{cKD} animals. In both of these models, reduced fibrosis was presumably related to non–TAK1-dependent signaling such as Smad-regulated signaling in nonmyocytes,

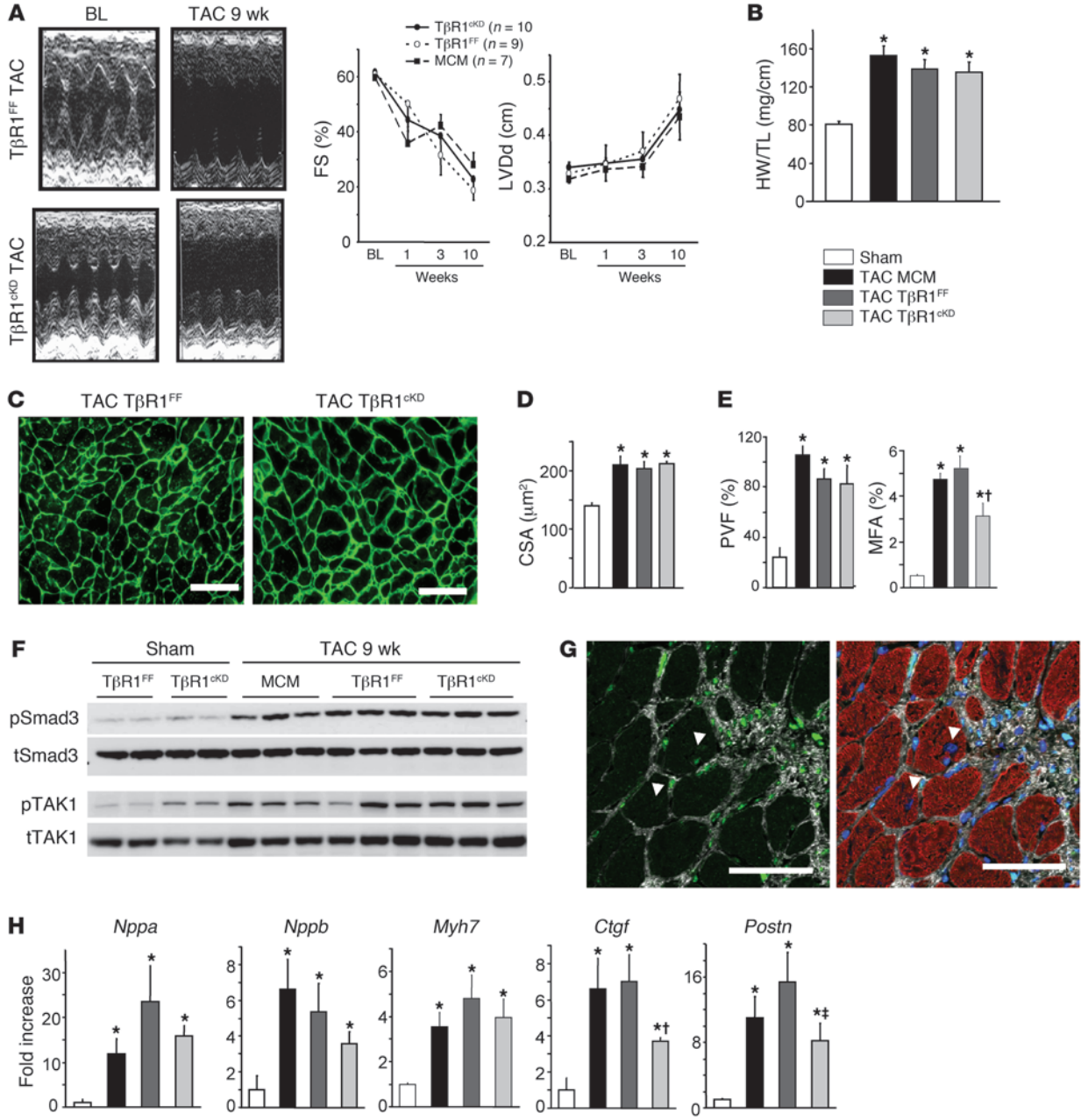

Figure 7

Cardiomyocyte TβR1 knockdown does not prevent cardiac hypertrophy and remodeling in response to pressure overload. (**A**). Representative M-mode echocardiogram after TAC, and temporal changes of FS and LV diastolic dimension. (**B**–**D**). Cardiac hypertrophy was not inhibited in TβR1^{cKD} animals. *P < 0.05 vs. sham. (**B**) Heart weight/tibia length ratio. n = 8 (sham); 11 (TAC MCM); 9 (TAC TβR1^{FF}); 10 (TAC TβR1^{cKD}). (**C**) Representative WGA staining for CSA measurement. Scale bars: 50 μm. (**D**) Myocyte hypertrophy, as assessed by CSA. Averaged data from 400–800 cells per heart. n = 4 (sham); 7 (TAC MCM), 5 (TAC TβR1^{FF} and TAC TβR1^{cKD}). (**E**) Reduced myocardial but not perivascular fibrosis area in TβR1^{cKD} mice. n = 4 (sham); 7 (TAC MCM), 5 (TAC TβR1^{FF} and TAC TβR1^{cKD}). *P < 0.05 vs. sham; †P < 0.05 vs. TAC TβR1^{FF}. (**F**) Representative Western blot for Smad3 and TAK1 activation after TAC. (**G**) Representative phospho-Smad3 immunostaining in LV after 9-week TAC in TβR1^{cKD}. Green, phospho-Smad3; red, sarcomeric α-actinin; blue, DAPI; white, WGA. White arrowheads, cardiomyocyte Smad3 activation. Scale bars: 50 μm. (**H**) mRNA expression levels, normalized to *Gapdh* and then to sham data, assessed by real-time RT-PCR. n = 7 (sham); 4 (TAC MCM); 5 (TAC TβR1^{FF}); 8 (TAC TβR1^{cKD}). *P < 0.05 vs. sham; †P < 0.05 vs. TAC TβR1^{FF}; ‡P < 0.05 vs. TAC MCM.

periostin, and other secreted proteins. Direct proof of the central role of TAK1 to these cascades in vivo awaits development of a suitable inhibitor, as genetic models would involve very complex dually inducible systems. Proof of the effect of *Bmp7* changes mediated by myocyte TβR2 on fibrosis and/or vascularity in vivo will also require further studies.

Another major finding in the current study was identification of the central role of myocyte TβR2-dependent signaling on

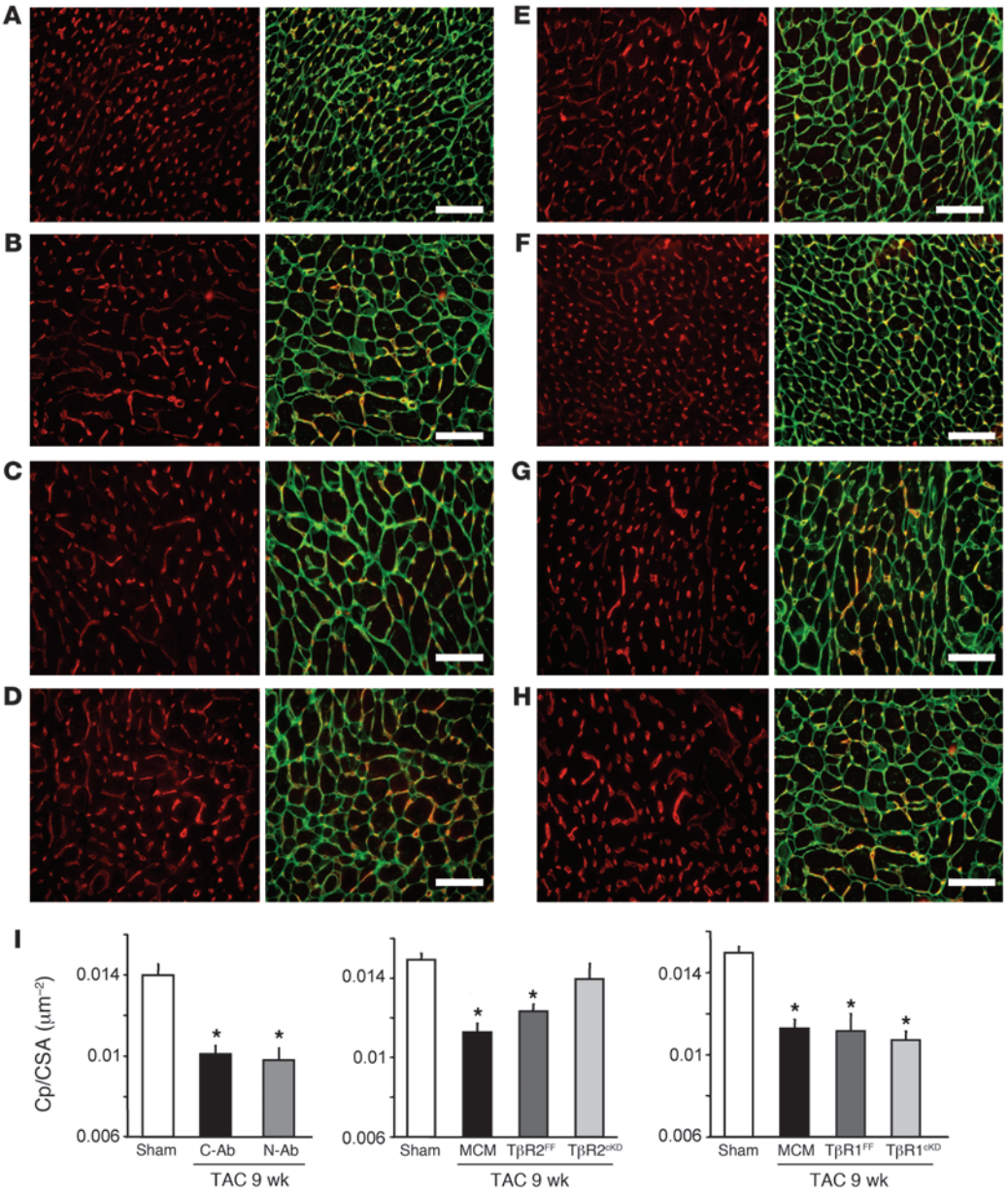

Figure 8

Hearts with suppressed TβR2 have preserved capillary density/myocyte area ratio. (**A**–**H**) Myocardium stained for endothelial calls (red, isolectin B4) or WGA (green) in (**A**) sham, (**B**) 9-week TAC plus C-Ab, (**C**) 9-week TAC plus N-Ab, (**D**) MCM with 9-week TAC, (**E**) $T\beta R2^{FF}$ with 9-week TAC, (**F**) $T\beta R2^{cKD}$ with 9-week TAC, (**G**) $T\beta R1^{FF}$ with 9-week TAC, and (**H**) $T\beta R1^{cKD}$ with 9-week TAC hearts. Scale bars: 50 μm. (**I**) Capillary density (Cp), normalized to myocyte CSA, declined after TAC, and was unaltered in N-Ab–treated and $T\beta R1^{cKD}$ hearts, but enhanced in $T\beta R2^{cKD}$ hearts. *$P < 0.05$ vs. sham.

TAC-induced pathological hypertrophy and dysfunction. Gene knockdown of Smad4 in cardiac myocytes leads to hypertrophy and cardiac failure (43), whereas deletion of Smad3 worsens the hypertrophic response to pressure overload (25). However, non-Smad pathways coupled to TGF-β signaling, particularly in myocytes, may orchestrate a more unified maladaptive response. This signaling includes ras-MEK, Rho GTPase, phosphoinositide-3-kinase, and TAK1 (14). We focused on TAK1 given its prominent expression in cardiomyocytes (29) and prior data showing that gene-targeted myocyte upregulation induces hypertrophy and heart failure (16). TAK1 activates p38 MAPK, and phosphorylation of both declined with $T\beta R2^{cKD}$ animals, but not $T\beta R1^{cKD}$ animals, consistent with differences in its modulation. This is likely important, as p38 MAPK activation itself induces cardiomyopathy with abnormal systolic and diastolic function and depresses the myofibrillar force response to calcium (44, 45). Although TAK1 activation was first identified as a TGF-β–activated kinase, it is also stimulated by inflammatory cytokines such as IL-1 and TNF-α through TNF-α receptor–associated factor–mediated (TRAF-mediated) lysine 63–linked polyubiquitination (46).

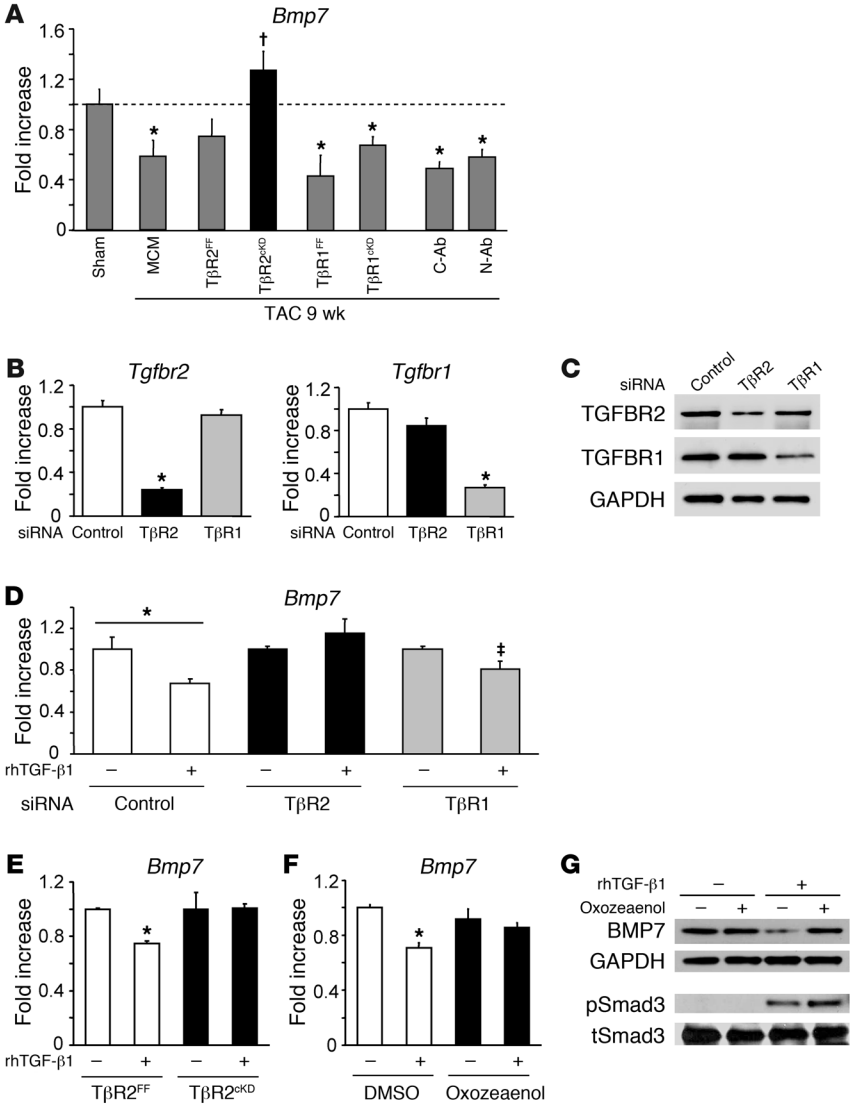

Figure 9

Suppression of myocyte TβR2 uniquely upregulated BMP7 through TAK1 signaling. (**A**) Myocardial gene expression of *Bmp7* declined after TAC in all groups except TβR2^{cKD}. *$P < 0.05$ vs. sham; †$P < 0.05$ vs. MCM and TβR2^{FF}. (**B** and **C**) Gene knockdown by TβR2 or TβR1 siRNA transfection in cultured neonatal rat cardiomyocytes. (**B**) *Tgfbr2* and *Tgfbr1* mRNA levels, normalized to *Gapdh* and then to control siRNA, as assessed by real-time RT-PCR. $n = 4$ per group. *$P < 0.05$ vs. control. (**C**) Representative Western blot for TβR2 or TβR1. (**D**) TGF-β1–mediated downregulation of *Bmp7* was more effectively blocked by TβR2 siRNA than by TβR1 siRNA. rhTGF-β1 was administered at 5 ng/ml for 24 hours. *$P < 0.05$ as indicated; ‡$P < 0.05$, 2-way ANOVA, for interaction of siRNA and rhTGF-β1 effect. (**E**–**G**) BMP7 expression in cultured adult mouse cardiomyocytes. TGF-β–mediated *Bmp7* mRNA downregulation was blunted in TβR2^{cKD} animals (**E**) and by pretreatment with the TAK1 inhibitor oxozeaenol (50 nM; **F**). *$P < 0.05$ vs. respective rhTGF-β1–unstimulated control. (**G**) Western blot for BMP7 using cultured adult mouse cardiomyocytes. Oxozeaenol prevented BMP7 decrease at the protein level, independent of Smad3 activation.

TRAF6 is also involved with TGF-β–mediated TAK1 activation, with studies suggesting this occurs in a TβR1 kinase–dependent (47) or –independent manner (48). This could have contributed to TAK1 activation in TβR1^{cKD} mice.

In conclusion, myocyte-targeted noncanonical TGF-β signaling plays a central role in the maladaptive cardiac response to sustained pressure overload. Our results highlighted benefits of inhibiting non–Smad-dependent pathways, in particular TAK1. Canonical Smad-dependent signaling played a major role in cardiac fibrosis, yet its suppression was insufficient to ameliorate chamber dysfunction and hypertrophy and, if selectively targeted, may even worsen cardiac pathophysiology. It is possible that alternative pathophysiologic stimuli, such as angiotensin or β-adrenergic stimulation, myocardial infarction, and inflammatory myocarditis may involve cell-specific TGF-β signaling different from that found in pressure overload. This could alter the relative role of downstream cascades and cell types. The present data revealed the complexity of such signaling and suggest that cell-selective targeting of anti–TGF-β strategies may indeed be required to optimally leverage this approach.

Methods

Mice. Male C57BL/6 mice (8–11 weeks, Jackson Laboratories) were used in the N-Ab studies. The N-Ab 1D11 and the C-Ab 13C4 were both provided by Genzyme. Ab treatment was initiated on the day of TAC surgery by intraperitoneal injection (5 mg/kg BW, 3× per week; refs. 24, 28). Myocyte-targeted inducible transgenic mice were generated as previously described (32). *Myh6*-MCM$^{+/+}$ transgenic mice (B6/129-tg[*Myh6*-cre/Esr1]1Jmk/J; stock no. 005650; The Jackson Laboratory) were crossed with C57BL/6 mice to generate *Myh6*-MCM$^{+/-}$ no-flox animals (MCM). These in turn were crossed with either *Tgfbr2*$^{fl/fl}$ mice (provided by H.L. Moses, Vanderbilt University, Nashville, Tennessee, USA) or *Tgfbr1*$^{fl/fl}$ mice (both on C57BL/6 background) to derive *Myh6*-MCM$^{+/-}$*Tgfbr2*$^{fl/fl}$ (TβR2^{cKD}) or *Myh6*-MCM$^{+/-}$*Tgfbr1*$^{fl/fl}$ (TβR1^{cKD}) mice, respectively. Genotype was confirmed with primers to *Cre* and *Tgfbr2* or *Tgfbr1* floxed alleles (32). To induce recombination, tamoxifen citrate (Sigma-Aldrich) was mixed in soft diet (Bioserve), with daily intake approximately 4 g/d, mixing 500 mg tamoxifen per 1 kg food to provide a net 80 mg/kg/d, administered daily for 7 days. Confirmation of gene knockdown in both models has been previously reported (32), and protein reduction is shown in Supplemental Figure 1C. All MCM-positive transgene–carrying mice developed transient cardiomyopathy, but fully recovered 3 weeks after

stopping tamoxifen. Experiments were started after confirmation of functional recovery by echocardiography. Whereas our prior report suggested the myopathy could be avoided by using raloxifene (32), we ultimately found gene knockdown was insufficiently consistent with this approach.

TAC. Pressure overload was produced by constricting the transverse aorta as previously described (26). The aorta was approached via minimal sternal incision and a 7-0 ligature placed around the vessel using a 26-gauge needle to ensure consistent occlusion. Sham-operated mice underwent the same surgery without constriction. The protocol was approved by the Johns Hopkins Medical Institutions Animal Care and Use Committee.

Echocardiography. In vivo cardiac morphology was assessed by transthoracic echocardiography (Acuson Sequoia C256, 13MHz transducer; Siemens) in conscious mice. M-mode LV end-systolic and end-diastolic dimensions were averaged from 3–5 beats. LV percent FS and mass were calculated as described previously (26, 27). The studies and analysis were performed blinded as to experimental group.

In vivo hemodynamics. In vivo LV function was assessed by PV catheter, as described previously (49). Mice were anesthetized, intubated, and ventilated. The LV apex was exposed between the seventh and eighth ribs, and a 1.4-Fr PV catheter (SPR 839; Millar Instruments Inc.) was advanced through the apex to lie along the longitudinal axis. Absolute volume was determined by saline calibration and ultrasound aortic, and data were assessed at steady state and during preload reduction. Data were digitized at 2 kHz and analyzed with custom software.

Western blot. Protein analysis was performed using standard techniques. LV tissues were dissected from mouse heart and homogenized with lysis buffer (Cell Signaling Technology), and lysates were subjected to Western blot using a NuPage system (Invitrogen) and probed with phospho-Smad2/3 (p423/425) or phospho-TAK1 (T184/187) Abs (Cell Signaling). Membranes were then reprobed with total Smad2/3 or TAK1 Abs (Cell Signaling). Band intensity was quantified by NIH Image J software. Phosphorylated and total p38 MAPK Abs and GAPDH Abs were purchased from Cell signaling. TβR2 and TβR1 Abs were from Santa Cruz.

RNA analysis. Total RNA was prepared, using TRIzol reagent (Invitrogen), from LV tissue or isolated myocytes. mRNA was analyzed by quantitative real-time PCR using either SYBR green or TaqMan probe method. Real-time PCR reactions were performed, recorded, and analyzed using ABI PRISM 7900 (Applied Biosystems). *Ctgf*, *Bmp7*, *Postn*, and *Gapdh* were assessed using specific primer-probe from Applied Biosystems. mRNA levels of *Nppa*, *Nppb*, *Myh7*, and *Gapdh* were quantified using SYBR green PCR primers as previously described (32). The specificity of the SYBR green assays was confirmed by dissociation curve analysis. To screen TGF-β/BMP-related gene expressions, we used PCR-based array system, mouse TGF-β/BMP signaling array (PAMM-035; SA Biosciences) according to the manufacturer's protocol.

Tissue histology. Myocardium fixed with 10% formalin was analyzed for myocyte hypertrophy and fibrosis. Tissue was paraffin embedded, sectioned into 10-μm slices, and stained with Masson trichrome to measure fibrosis. We analyzed 6 serial sections of mid-LV per heart. To assess angiogenic response for cardiomyocyte hypertrophy, tissue was costained with wheat germ agglutinin (WGA; plasma membrane staining, Alexa Fluor 488 conjugated) and isolectin B4 (GS-IB4; endothelial staining, Alexa Fluor 568 conjugated). The paraffin-embedded sections were treated with an antigen retrieval solution (Dako) and incubated with WGA and isolectin B4 at 4°C overnight. Cardiomyocyte cross-sectional area (CSA) and capillary density were measured from the same image with different fluorescence. The images were captured with fluorescence microscope and analyzed by iVision software. All histological quantifications were performed by 2 observers in a blinded manner. Data from 400–800 cells were determined per slide, using semiautomated edge detection software (iVision, version 4.01; BioVision Technologies).

Immunostaining and confocal microscopy. The paraffin-embedded sections were stained with rabbit anti–phospho-Smad3 Ab (S423/425; Millipore) using an Alexa Fluor 488–conjugated anti-rabbit TSA kit (Invitrogen) following the manufacturer's protocol. DAPI (Invitrogen), WGA (Alexa Fluor 647; Invitrogen), mouse anti-SMA Ab (DAKO), anti-vimentin Ab (Sigma-Aldrich), and anti–sarcomeric α-actinin Ab (Sigma-Aldrich) were used for counterstaining of nuclei, plasma membrane/extracellular matrix, vascular SMCs, fibroblasts, and myocytes, respectively. In some experiments, we used frozen heart tissue embedded in OCT compound to make cryosections. Cryosections were fixed with 10% formalin and used for immunostaining. Confocal analysis was performed on a Zeiss LSM510-META laser scanning confocal microscope (Johns Hopkins University Institute for Basic Biomedical Sciences Microscopy Facility).

Fluorescence-probed Ab treatment and analysis. Alexa Fluor 555–conjugated 1D11 and 13C4 were provided by Genzyme. The Ab was delivered to mice 6–7 weeks after TAC by intraperitoneal injection (10 mg/kg BW). 24 hours after injection, hearts were harvested and frozen in OCT compound. Cryosections were immunofluorescently labeled for macrophages using a rat anti-mouse CD68 monoclonal primary Ab (Serotec) and Alexa Fluor 647–conjugated goat anti-rat IgG secondary Ab (Invitrogen). Some slides were stained using purified rat IgG in place of the CD68 primary Ab. All slides were counterstained with DAPI. Imaging was conducted using a Zeiss Mirax Scan automated widefield fluorescence slide scanner and a Zeiss LSM510-META laser scanning confocal microscope.

Cardiac myocytes cultured from neonatal rats, and RNA interference. Primary cultures of neonatal cardiac ventricular myocytes were prepared as previously described (50). For RNA interference analysis of TβR2 or TβR1, ON-TARGETplus SMART pool reagent against rat TGFBR2 (L-091837-01-0020) and rat TGFBR1 (L-098121-01-0020) were purchased from Dharmacon. ON-TARGETplus Non-targeting pool (Dharmacon) was used as a nonspecific control. 24 hours after plating, cells were transfected with 100 nM siRNAs using DharmaFECT 1 (Dharmacon) following the manufacturer's protocol. RNA or protein was harvested 24–48 hours after transfection.

Cardiac myocytes cultured from adult mice. Primary cultured ventricular myocytes isolated from adult mice were prepared using recently reported methods (50). Collagenase-digested isolated myocytes were incubated in buffer with increasing concentrations of Ca^{2+}, achieving a final concentration of 1.2 mM Ca^{2+} as in MEM culture media (Sigma-Aldrich). Cells were seeded at 25,000 rod-shaped myocytes/ml on 6-well plates or 60-mm dishes coated with laminin. After 1 hour incubation in 37°C, 5% CO_2, the culture media was replaced to remove unattached cells. After overnight culture, cells were stimulated with rhTGF-β1 (Sigma-Aldrich) with or without the TAK1 inhibitor 5Z-7-oxozeaenol (Sigma-Aldrich).

Statistics. All values are expressed as mean ± SEM. Group comparisons were performed by 1- or 2-way ANOVA or by nonpaired 2-tailed Student's *t* test. Sample sizes and individual statistical results for all analyses are provided in the figures, supplemental figures, and supplemental tables.

Acknowledgments

This study was supported by NIH grants HL-89297, HL-59408, HL-84946 (to D.A. Kass), and T32-HL-077180 (to D.A. Kass); by an American Heart Association Mid-Atlantic Fellowship Grant (to N. Koitabashi); and by the Japan Heart Foundation/Bayer Yakuhin Research Grant Abroad (to N. Koitabashi). The authors thank Harold L. Moses (Vanderbilt University) for originally providing the *Tgfbr2*$^{fl/fl}$ mice, Doug Matthews and Charlene Manning (Genzyme) for assistance with the fluorescence-labeled N-Ab experiments, Genzyme for providing N-Ab and C-Ab, and Djahida Bedja and Marissa Hildebrandt (Johns Hopkins Medical Institu-

tions) for their assistance with echocardiography and capillary density analysis, respectively.

Received for publication August 19, 2010, and accepted in revised form March 2, 2011.

Address correspondence to: David A. Kass, Division of Cardiology, Johns Hopkins Medical Institutions, Ross Research Building, Room 858, 720 Rutland Avenue, Baltimore, Maryland 21205, USA. Phone: 410.955.7153; Fax: 410.502.2558; E-mail: dkass@jhmi.edu.

1. Levy D, Garrison RJ, Savage DD, Kannel WB, Castelli WP. Prognostic implications of echocardiographically determined left ventricular mass in the Framingham Heart Study. *N Engl J Med*. 1990; 322(22):1561–1566.
2. Frey N, Olson EN. Cardiac hypertrophy: the good, the bad, and the ugly. *Annu Rev Physiol*. 2003;65:45–79.
3. Katz AM. Maladaptive growth in the failing heart: the cardiomyopathy of overload. *Cardiovasc Drugs Ther*. 2002;16(3):245–249.
4. Mudd JO, Kass DA. Tackling heart failure in the twenty-first century. *Nature*. 2008;451(7181):919–928.
5. Manabe I, Shindo T, Nagai R. Gene expression in fibroblasts and fibrosis: involvement in cardiac hypertrophy. *Circ Res*. 2002;91(12):1103–1113.
6. Swynghedauw B. Molecular mechanisms of myocardial remodeling. *Physiol Rev*. 1999;79(1):215–262.
7. Kakkar R, Lee RT. Intramyocardial fibroblast myocyte communication. *Circ Res*. 2010;106(1):47–57.
8. Souders CA, Bowers SL, Baudino TA. Cardiac fibroblast: the renaissance cell. *Circ Res*. 2009; 105(12):1164–1176.
9. Brand T, Schneider MD. The TGF beta superfamily in myocardium: ligands, receptors, transduction, and function. *J Mol Cell Cardiol*. 1995;27(1):5–18.
10. Hein S, et al. Progression from compensated hypertrophy to failure in the pressure-overloaded human heart: structural deterioration and compensatory mechanisms. *Circulation*. 2003;107(7):984–991.
11. Li RK, et al. Overexpression of transforming growth factor-beta1 and insulin-like growth factor-I in patients with idiopathic hypertrophic cardiomyopathy. *Circulation*. 1997;96(3):874–881.
12. Euler-Taimor G, Heger J. The complex pattern of SMAD signaling in the cardiovascular system. *Cardiovasc Res*. 2006;69(1):15–25.
13. Zeisberg EM, et al. Endothelial-to-mesenchymal transition contributes to cardiac fibrosis. *Nat Med*. 2007;13(8):952–961.
14. Derynck R, Zhang YE. Smad-dependent and Smad-independent pathways in TGF-beta family signalling. *Nature*. 2003;425(6958):577–584.
15. Rahimi RA, Leof EB. TGF-beta signaling: a tale of two responses. *J Cell Biochem*. 2007;102(3):593–608.
16. Zhang D, et al. TAK1 is activated in the myocardium after pressure overload and is sufficient to provoke heart failure in transgenic mice. *Nat Med*. 2000; 6(5):556–563.
17. Takahashi N, Calderone A, Izzo NJ Jr, Maki TM, Marsh JD, Colucci WS. Hypertrophic stimuli induce transforming growth factor-beta 1 expression in rat ventricular myocytes. *J Clin Invest*. 1994; 94(4):1470–1476.
18. Lim JY, et al. TGF-beta1 induces cardiac hypertrophic responses via PKC-dependent ATF-2 activation. *J Mol Cell Cardiol*. 2005;39(4):627–636.
19. Schultz JJ, et al. TGF-beta1 mediates the hypertrophic cardiomyocyte growth induced by angiotensin II. *J Clin Invest*. 2002;109(6):787–796.
20. Cohn RD, et al. Angiotensin II type 1 receptor blockade attenuates TGF-beta-induced failure of muscle regeneration in multiple myopathic states. *Nat Med*. 2007;13(2):204–210.
21. Habashi JP, et al. Losartan, an AT1 antagonist, prevents aortic aneurysm in a mouse model of Marfan syndrome. *Science*. 2006;312(5770):117–121.
22. Kuwahara F, et al. Transforming growth factor-beta function blocking prevents myocardial fibrosis and diastolic dysfunction in pressure-overloaded rats. *Circulation*. 2002;106(1):130–135.
23. Sakata Y, Chancey AL, Divakaran VG, Sekiguchi K, Sivasubramanian N, Mann DL. Transforming growth factor-beta receptor antagonism attenuates myocardial fibrosis in mice with cardiac-restricted overexpression of tumor necrosis factor. *Basic Res Cardiol*. 2008;103(1):60–68.
24. Frantz S, et al. Transforming growth factor beta inhibition increases mortality and left ventricular dilatation after myocardial infarction. *Basic Res Cardiol*. 2008;103(5):485–492.
25. Divakaran V, et al. Adaptive and maladptive effects of SMAD3 signaling in the adult heart after hemodynamic pressure overloading. *Circ Heart Fail*. 2009; 2(6):633–642.
26. Takimoto E, et al. Chronic inhibition of cyclic GMP phosphodiesterase 5A prevents and reverses cardiac hypertrophy. *Nat Med*. 2005;11(2):214–222.
27. Nagayama T, et al. Sildenafil stops progressive chamber, cellular, and molecular remodeling and improves calcium handling and function in hearts with pre-existing advanced hypertrophy caused by pressure overload. *J Am Coll Cardiol*. 2009;53(2):207–215.
28. Dasch JR, Pace DR, Waegell W, Inenaga D, Ellingsworth L. Monoclonal antibodies recognizing transforming growth factor-beta. Bioactivity neutralization and transforming growth factor beta 2 affinity purification. *J Immunol*. 1989;142(5):1536–1541.
29. Matsumoto-Ida M, Takimoto Y, Aoyama T, Akao M, Takeda T, Kita T. Activation of TGF-beta1-TAK1-p38 MAPK pathway in spared cardiomyocytes is involved in left ventricular remodeling after myocardial infarction in rats. *Am J Physiol Heart Circ Physiol*. 2006;290(2):H709–H715.
30. Koitabashi N, et al. Increased connective tissue growth factor relative to brain natriuretic peptide as a determinant of myocardial fibrosis. *Hypertension*. 2007;49(5):1120–1127.
31. Snider P, Standley KN, Wang J, Azhar M, Doetschman T, Conway SJ. Origin of cardiac fibroblasts and the role of periostin. *Circ Res*. 2009; 105(10):934–947.
32. Koitabashi N, et al. Avoidance of transient cardiomyopathy in cardiomyocyte-targeted tamoxifen-induced MerCreMer gene deletion models. *Circ Res*. 2009;105(1):12–15.
33. Oshima M, Oshima H, Taketo MM. TGF-beta receptor type II deficiency results in defects of yolk sac hematopoiesis and vasculogenesis. *Dev Biol*. 1996;179(1):297–302.
34. Hu PP, Shen X, Huang D, Liu Y, Counter C, Wang XF. The MEK pathway is required for stimulation of p21(WAF1/CIP1) by transforming growth factor-beta. *J Biol Chem*. 1999;274(50):35381–35387.
35. Watkins SJ, Jonker L, Arthur HM. A direct interaction between TGFbeta activated kinase 1 and the TGFbeta type II receptor: implications for TGFbeta signalling and cardiac hypertrophy. *Cardiovasc Res*. 2006;69(2):432–439.
36. Sano M, et al. p53-induced inhibition of Hif-1 causes cardiac dysfunction during pressure overload. *Nature*. 2007;446(7134):444–448.
37. Wang S, Hirschberg R. Bone morphogenetic protein-7 signals opposing transforming growth factor beta in mesangial cells. *J Biol Chem*. 2004; 279(22):23200–23206.
38. Oxburgh L. Control of the bone morphogenetic protein 7 gene in developmental and adult life. *Curr Genomics*. 2009;10(4):223–230.
39. Leask A. Potential therapeutic targets for cardiac fibrosis: TGFbeta, angiotensin, endothelin, CCN2, and PDGF, partners in fibroblast activation. *Circ Res*. 2010;106(11):1675–1680.
40. Matsui Y, Sadoshima J. Rapid upregulation of CTGF in cardiac myocytes by hypertrophic stimuli: implication for cardiac fibrosis and hypertrophy. *J Mol Cell Cardiol*. 2004;37(2):477–481.
41. Yoon PO, et al. The opposing effects of CCN2 and CCN5 on the development of cardiac hypertrophy and fibrosis. *J Mol Cell Cardiol*. 2010;49(2):294–303.
42. David L, Feige JJ, Bailly S. Emerging role of bone morphogenetic proteins in angiogenesis. *Cytokine Growth Factor Rev*. 2009;20(3):203–212.
43. Wang J, et al. Targeted disruption of Smad4 in cardiomyocytes results in cardiac hypertrophy and heart failure. *Circ Res*. 2005;97(8):821–828.
44. Liao P, et al. The in vivo role of p38 MAP kinases in cardiac remodeling and restrictive cardiomyopathy. *Proc Natl Acad Sci U S A*. 2001;98(21):12283–12288.
45. Vahebi S, et al. p38-MAPK induced dephosphorylation of alpha-tropomyosin is associated with depression of myocardial sarcomeric tension and ATPase activity. *Circ Res*. 2007;100(3):408–415.
46. Adhikari A, Xu M, Chen ZJ. Ubiquitin-mediated activation of TAK1 and IKK. *Oncogene*. 2007; 26(22):3214–3226.
47. Yamashita M, Fatyol K, Jin C, Wang X, Liu Z, Zhang YE. TRAF6 mediates Smad-independent activation of JNK and p38 by TGF-beta. *Mol Cell*. 2008; 31(6):918–924.
48. Sorrentino A, et al. The type I TGF-beta receptor engages TRAF6 to activate TAK1 in a receptor kinase-independent manner. *Nat Cell Biol*. 2008; 10(10):1199–1207.
49. Pacher P, Nagayama T, Mukhopadhyay P, Batkai S, Kass DA. Measurement of cardiac function using pressure-volume conductance catheter technique in mice and rats. *Nat Protoc*. 2008;3(9):1422–1434.
50. Koitabashi N, et al. Cyclic GMP/PKG-dependent inhibition of TRPC6 channel activity and expression negatively regulates cardiomyocyte NFAT activation Novel mechanism of cardiac stress modulation by PDE5 inhibition. *J Mol Cell Cardiol*. 2010;48(4):713–724.